

PDE Evolutions for M-Smothers: From Common Myths to Robust Numerics

Martin Welk¹ and Joachim Weickert²

¹ Institute of Biomedical Image Analysis
Private University of Health Sciences, Medical Informatics and Technology
Eduard-Wallnöfer-Zentrum 1, 6060 Hall/Tyrol, Austria
martin.welk@umit.at

² Mathematical Image Analysis Group, Campus E1.7
Saarland University, 66041 Saarbrücken, Germany
weickert@mia.uni-saarland.de

Abstract. Local M-smoothers constitute an interesting and important class of image processing techniques with many connections to other methods. In our paper we derive a family of partial differential equations (PDEs) that result as limiting processes from M-smoothers which are based on local order- p means within a disc the radius of which tends to zero. The order p may take any nonzero value > -1 . Thus, we also allow negative values which have never been considered before. In contrast to results from the literature, we show in the space-continuous case that mode filtering does not arise for $p \rightarrow 0$, but for $p \rightarrow -1$. Extending our filter class to p -values smaller than -1 allows to include e.g. the classical image sharpening flow of Gabor. Since our PDE class is highly anisotropic and may contain backward parabolic operators, designing adequate numerical methods is difficult. We present an L^∞ -stable explicit finite difference scheme that satisfies a discrete maximum–minimum principle, is fairly efficient, and offers excellent rotation invariance. Although it solves parabolic PDEs, it makes consequent use of stabilisation concepts from the numerics of hyperbolic PDEs. Our experiments show that the PDEs for $p < 1$ are of specific interest: Their backward parabolic term creates favourable sharpening properties, while they appear to maintain the strong shape simplification properties of mean curvature motion.

Keywords: M-smoother · partial differential equation · mode filter · backward parabolic operator · anisotropy · finite difference methods · shape analysis

1 Introduction

M-estimators. It has been observed long ago by Legendre [15] and Gauß [8] that the mean of a finite multiset $\mathcal{X} = \{a_1, a_2, \dots, a_n\}$ of real numbers can be described as the minimiser of the sum of squared distances to the given numbers:

$$\text{mean}(\mathcal{X}) = \operatorname{argmin}_{\mu \in \mathbb{R}} \sum_{i=1}^n (\mu - a_i)^2. \quad (1)$$

Likewise it has been noted by Jackson [13] that the median of \mathcal{X} minimises the sum of absolute distances:

$$\text{median}(\mathcal{X}) = \operatorname{argmin}_{\mu \in \mathbb{R}} \sum_{i=1}^n |\mu - a_i|. \quad (2)$$

This can be generalised to the notion of *order- p means* given by

$$\text{mean}_p(\mathcal{X}) := \operatorname{argmin}_{\mu \in \mathbb{R}} \sum_{i=1}^n |\mu - a_i|^p \quad (3)$$

for any $p > 0$, with $\text{mean}_2 \equiv \text{mean}$, $\text{mean}_1 \equiv \text{median}$. This concept is introduced by Jackson [13] for $p > 1$ (as a means to disambiguate the median by $p \rightarrow 1^+$) whereas Barral Souto [2] is interested in the order- p means in their own right for general $p > 0$. In robust statistics, order- p means belong to the class of *M-estimators* [12].

Including the limiting case of the monomials as $|z|^0 = 0$ for $z = 0$, and 1 otherwise, [2] also extends the definition (3) to the case $p = 0$ for which the *mode* of \mathcal{X} , i.e. its most frequent value, is obtained. As also noted in [2], the limit $p \rightarrow \infty$ yields what is also called the mid-range value, i.e. the arithmetic mean of the extremal values of \mathcal{X} .

It is straightforward to rewrite the definition of order- p means for continuous distributions (densities) on \mathbb{R} just by replacing sums with integrals: Let $\gamma : \mathbb{R} \rightarrow \mathbb{R}_0^+$ be a density (integrable in a suitable sense), then one defines

$$\text{mean}_p(\gamma) := \operatorname{argmin}_{\mu \in \mathbb{R}} \int_{-\infty}^{\infty} \gamma(z) |\mu - z|^p dz. \quad (4)$$

This notion of continuous order- p means has been considered by Fréchet [6] for $p > 1$.

M-smoothers. In image processing, M-estimators are commonly used to build local image filters, see [22] for the median filter (in signal processing) and [21] for order- p means with $p > 0$. In a local filter, one takes at each location the greyvalues from a neighbourhood (selection step) and computes some common value of these (aggregation step) that is assigned to the location in the filtered signal, see e.g. [5, 9]. These filters can be iterated to generate a series of progressively processed images.

It has been noticed since long that these filters behave similar to certain image filters based on partial differential equations (PDEs). Mean filters are a spatial discretisation of linear diffusion. As proven in [11], iterated median filtering approximates mean curvature motion [1]. In [9], also the case of the mode filter (associated with $p = 0$) is considered.

Our contribution. We derive a family of PDEs associated with M-smoothers based on order- p means with variable p and vanishing disc radius. In contrast to results from the literature, we also permit negative p -values with $p > -1$. Reconsidering the relation of order- p means and their corresponding PDEs to existing image filters, we show that in the space-continuous setting the mode filter does *not* arise for $p \rightarrow 0$, as is commonly assumed [9], but for $p \rightarrow -1$. Extending our PDE family to values $p < -1$ allows to cover also the sharpening Gabor flow [7, 16], for which no M-smoothing counterpart is known. In spite of the fact that our PDE family is anisotropic and may even involve

backward parabolic operators, we design an L^∞ -stable numerical scheme with very good rotation invariance. Our experiments show that the PDEs for $p < 1$ are particularly attractive since they simultaneously allow image sharpening and shape simplification.

Structure of the paper. In Section 2 we present our theory that allows us to derive PDE evolutions from M-smoothers. Our numerical algorithm is discussed in Section 3, and Section 4 is devoted to an experimental evaluation. Our paper is concluded with a summary in Section 5.

2 M-Smootherers, Mode and Partial Differential Equations

In this section, we derive PDEs for M-smoothers and the mode filter.

Generalised order- p means. In the following, M-smoothers are based on order- p means with $p > -1$, $p \neq 0$. As this range for p goes beyond the usual $p > 0$, let us first extend the definition of order- p means of continuous-scale distributions accordingly.

Definition 1. *Let z be a real random variable with the bounded, piecewise continuous density $\gamma : \mathbb{R} \rightarrow \mathbb{R}$. For $p \in (-1, +\infty) \setminus \{0\}$, define the order- p mean of γ as*

$$\text{mean}_p(\gamma) = \underset{\mu \in \mathbb{R}}{\text{argmin}} \int_{\mathbb{R}} \gamma(z) \text{sgn}(p) |\mu - z|^p dz . \quad (5)$$

As $|z|^p$ is monotonically increasing on \mathbb{R}_0^+ for $p > 0$, but monotonically decreasing on \mathbb{R}^+ for $p < 0$, the $\text{sgn}(p)$ factor in (5) ensures that in both cases an increasing penalty function is used.

For $p > 0$ the requirement of continuity of γ in Def. 1 can be relaxed; by modelling a discrete density as a weighted sum of delta peaks, the discrete order- p means as in [2] can be included in this definition.

The continuity is, however, essential for $p < 0$: In this case, the penalty function has a pole at $z = 0$ such that an improper integral is obtained; for $p > -1$ this integral exists provided that γ is continuous, i.e. no delta peaks are allowed. In particular, we cannot define an order- p mean with $-1 < p < 0$ for discrete distributions as considered in [2].

PDE approximation results. The proofs of the following propositions are given at the end of this section. The first proposition contains our first main result.

Proposition 1. *Let a smooth image $u : \mathbb{R}^2 \rightarrow \mathbb{R}$ be given, and let $\mathbf{x}_0 = (x_0, y_0)$ be a regular point, $|\nabla u(\mathbf{x}_0)| > 0$. One step of order- p mean filtering of u with a disc-shaped window $D_\varrho(\mathbf{x})$ and $p > -1$, $p \neq 0$ approximates for $\varrho \rightarrow 0$ a time step of size $\tau = \varrho^2 / (2p + 4)$ of an explicit time discretisation of the PDE*

$$u_t = u_{\xi\xi} + (p - 1) u_{\eta\eta} \quad (6)$$

where η and ξ are geometric coordinates referring at each image location to the direction of the positive gradient, and the level-line direction, respectively:

$$\begin{aligned} & \text{mean}_p\{u(x, y) \mid (x, y) \in D_\varrho(x_0, y_0)\} - u(x_0, y_0) \\ &= \frac{\varrho^2}{2(p+2)} (u_{\xi\xi}(x_0, y_0) + (p-1)u_{\eta\eta}(x_0, y_0)) + \mathcal{O}(\varrho^{(\min\{p,0\}+5)/2}). \end{aligned} \quad (7)$$

At a local minimum (maximum) of u , i.e. \mathbf{x}_0 with $|\nabla u(\mathbf{x}_0)| = 0$ where the Hessian $\mathbf{D}^2 u(\mathbf{x}_0)$ is positive (negative) semidefinite, the same filtering step fulfils for $\varrho \rightarrow 0$ the inequality $\text{mean}_p\{u(x, y) \mid (x, y) \in D_\varrho(x_0, y_0)\} - u(x_0, y_0) \geq 0$ (≤ 0), thus approximates an evolution $u_t \geq 0$ ($u_t \leq 0$).

The approximation order in (7) is $\mathcal{O}(\varrho^{1/2})$ for positive p but reduces to $\mathcal{O}(\varrho^{(p+1)/2})$ for negative p .

For $p = 2$ and $p = 1$ the proposition yields the same PDEs as [9] except for a time rescaling which is due to the choice of a Gaussian window in [9].

Under analogous assumptions as in Prop. 1, one can also derive the PDE limit for the mode filter, where the mode is not obtained by a minimisation in the sense of (4) but directly as the maximum of the density of values in $\{u(x, y) \mid (x, y) \in D_\varrho(x_0, y_0)\}$.

Proposition 2. *Let u and \mathbf{x} be as in Proposition 1. One step of mode filtering of u with a disc-shaped window $D_\varrho(\mathbf{x})$ approximates for $\varrho \rightarrow 0$ a time step of size $\tau = \varrho^2/2$ of an explicit time discretisation of the PDE $u_t = u_{\xi\xi} - 2u_{\eta\eta}$ with ξ, η as in Proposition 1. At a local minimum (maximum), mode filtering approximates $u_t \geq 0$ ($u_t \leq 0$).*

The PDE for mode filtering coincides with the one given in [9], again up to time rescaling. We see, however, that (7) for $p \rightarrow 0$ does not yield the PDE from Proposition 2 but $u_t = u_{\xi\xi} - u_{\eta\eta}$. Instead, the mode filtering PDE is obtained for $p \rightarrow -1$. Inserting $p = -2$ into (7) yields $u_t = u_{\xi\xi} - 3u_{\eta\eta}$ which was stated as an image sharpening PDE in [7, 16].

Proof (of Prop. 1). Assume w.l.o.g. that the regular location is $\mathbf{x}_0 = \mathbf{0} = (0, 0)$ with $u(0, 0) = 0$, and that the gradient of u at $(0, 0)$ is in the positive x direction, i.e. $u_x > 0$, $u_y = 0$. Setting $\alpha = u_x > 0$ and substituting $x = \varrho\xi$, $y = \varrho\eta$, $u(x, y) = \varrho\alpha\omega(\xi, \eta)$, we can use Taylor expansion of ω up to third order to write for $(\xi, \eta) \in D_1 \equiv D_1(\mathbf{0})$

$$\omega(\xi, \eta) = \xi + \beta\xi^2\varrho + \gamma\xi\eta\varrho + \delta\eta^2\varrho + \varepsilon_0\xi^3\varrho^2 + \varepsilon_1\xi^2\eta\varrho^2 + \varepsilon_2\xi\eta^2\varrho^2 + \varepsilon_3\eta^3\varrho^3 + \mathcal{O}(\varrho^3). \quad (8)$$

The sought M-smoother value $\mu = \varrho^2\alpha\kappa$ then corresponds to an extremum (minimum for $p > 0$, maximum for $p < 0$) of an integral in the unit disc D_1 ,

$$E(\kappa) = \iint_{D_1} |\omega - \kappa\varrho|^p d\eta d\xi \quad (9)$$

For sufficiently small ϱ , this integral can be rewritten as

$$E(\kappa) = \int_{-1}^1 W(\xi) |\omega(\xi, 0) - \kappa\varrho|^p d\xi + \mathcal{O}(\varrho^3). \quad (10)$$

Herein, $W(\xi)$ essentially consists for each ξ of an integral along the level line of ω going through $(\xi, 0)$. This integral measures the density of the value $\omega(\xi, 0)$ in the overall distribution of ω values within D_1 . Describing the level line by a function $\tilde{\xi}(\eta)$ on $[\eta_-^*(\xi), \eta_+^*(\xi)]$ where η_{\pm}^* correspond to its end points on the boundary of D_1 , $W(\xi)$ reads as

$$W(\xi) = \frac{\partial \omega}{\partial \xi}(\xi, 0) V(\xi), \quad V(\xi) = \int_{\eta_-^*(\xi)}^{\eta_+^*(\xi)} \left(\frac{\partial \omega}{\partial \xi}(\tilde{\xi}(\eta), \eta) \right)^{-1} d\eta. \quad (11)$$

By straightforward but lengthy calculations one obtains

$$\begin{aligned} \tilde{\xi}(\eta) &= \xi - (\gamma\xi + \delta\eta)\eta\varrho \\ &\quad + ((2\beta\xi + \gamma\eta)(\gamma\xi + \delta\eta) - \varepsilon_1\xi^2 - \varepsilon_2\xi\eta - \varepsilon_3\eta^2)\eta\varrho^2 + \mathcal{O}(\varrho^3), \end{aligned} \quad (12)$$

$$\eta_{\pm}^* = \pm\sqrt{1 - \xi^2} + (\gamma\xi^2 \pm \delta\xi\sqrt{1 - \xi^2})\varrho + (\chi(\xi) \pm \psi(\xi)\sqrt{1 - \xi^2})\varrho^2 + \mathcal{O}(\varrho^3) \quad (13)$$

where $\psi(\xi) = \psi_0 + \psi_1\xi + \psi_2\xi^2 + \psi_3\xi^3$ and $\chi(\xi)$ are polynomials in ξ of order 3 and 4, respectively, the exact coefficients of which are not further needed. Putting things together, one finds

$$W(\xi) = \left((w_{0,0} + w_{0,2}\varrho^2) + w_{1,0}\xi + w_{2,0}\varrho^2\xi^2 + w_{3,0}\varrho^2\xi^3 \right) \sqrt{1 - \xi^2} + \mathcal{O}(\varrho^3) \quad (14)$$

with

$$\begin{aligned} w_{0,0} &= 2, & w_{0,2} &= \frac{4}{3}\beta\delta + \frac{2}{3}\gamma^2 - \frac{2}{3}\varepsilon_2 + 2\psi_0, & w_{1,0} &= 2\delta + 2\psi_1\varrho, \\ w_{2,0} &= -2\gamma^2 - \frac{4}{3}\beta\delta - \frac{2}{3}\gamma^2 + \frac{2}{3}\varepsilon_2 + 2\psi_2, & w_{3,0} &= 2\psi_3. \end{aligned} \quad (15)$$

To evaluate the outer integral (10), its integration interval $[-1, 1]$ is split into four parts

$$E(\kappa) = \left(\int_{-1}^{-\sqrt{\varrho}} + \int_{-\sqrt{\varrho}}^{\nu\varrho} + \int_{\nu\varrho}^{\sqrt{\varrho}} + \int_{\sqrt{\varrho}}^1 \right) W(\xi) |\omega(\xi, 0) - \kappa\varrho|^p d\xi + \mathcal{O}(\varrho^3) \quad (16)$$

where $\omega(\nu\varrho) = \kappa\varrho$. Herein, the modulus in the integrand can be resolved to $\pm(\omega(\xi, 0) - \kappa\varrho)$ in each part. Substituting further ξ to $-\xi$, $-\xi + \nu\varrho$, $\xi - \nu\varrho$, ξ , respectively, in the four intervals, all integrals can be reduced up to higher order terms to combinations of standard integrals $\int \xi^q d\xi$ (in the inner two intervals) or $\int \xi^q \sqrt{1 - \xi^2} d\xi$ (in the outer two intervals) with several q , and by combining all these one arrives at

$$\begin{aligned} E(\kappa) &= \text{const}(\kappa) + \mathcal{O}(\varrho^{\min\{(p+5)/2, 5/2\}}) \\ &\quad + \left(-\frac{4p(p-1)}{p+1}\beta\varrho^2 S - \frac{2p}{p+1}\delta\varrho^2 S \right) \kappa + \left(\frac{2(p+2)p}{p+1}\varrho^2 S \right) \kappa^2 \end{aligned} \quad (17)$$

where the common constant S is defined by the definite integral

$$S = \int_{\arcsin \sqrt{\varrho}}^{\pi/2} \sin^{p+2} \varphi d\varphi. \quad (18)$$

The apex of the quadratic function in (17) yields the desired extremum of E , which is indeed a minimum for $p > 0$ and a maximum for $p < 0$:

$$\kappa = \frac{p-1}{p+1}\beta + \frac{1}{p+1}\delta + \mathcal{O}(\varrho^{(\min\{p,0\}+1)/2}). \quad (19)$$

Reverting our initial substitutions yields the claim of the proposition for regular points.

The inequalities for local minima (maxima) are obvious consequences of the fact that for any $\varrho > 0$ the mean- p filter value is in the convex hull of values $u(\mathbf{x})$, $\mathbf{x} \in D_\varrho(\mathbf{x}_0)$. \square

Proof (of Prop. 2). With the same substitutions as in the previous proof, the mode of ω is given by the maximiser of $V(\xi)$. By a slight modification of the calculations of the previous proof one finds

$$V(\xi) = 2(1 + \delta\xi\varrho - 2\beta\xi\varrho)\sqrt{1 - \xi^2} + \mathcal{O}(\xi^2\varrho^2). \quad (20)$$

Equating $V'(\xi)$ to zero yields $\omega(\xi) = (\delta - 2\beta)\varrho + \mathcal{O}(\varrho^2)$ for the mode. For local minima (maxima), the same reasoning as in the previous proof applies. \square

PDE evolutions. Propositions 1 and 2 state PDEs approximated by the respective M-smoothers at regular points, and inequalities that are valid at local minima and maxima. Let us briefly discuss how these results determine uniquely the evolutions of the entire image u (including critical points) approximated by the M-smoothers. To this end, notice first that in a connected critical region (a closed set in \mathbb{R}^2 consisting entirely of critical points, with nonempty interior), the inequalities for minima and maxima together imply $u_t = 0$.

An isolated critical point or a curve consisting of critical points, in contrast, is under the influence of the regular points surrounding it, and as long as the sign of the evolution speed u_t at the critical point and the surrounding regular points is of the same sign, the critical point will by a “sliding regime” be forced to adapt to the evolution speed of its regular surrounds. (A more detailed analysis will be given in a forthcoming paper.) If, however, the speed at the critical point is of opposite sign compared to all its surrounding regular points, they will coalesce to create a growing plateau which by the above remarks locks in at $u_t = 0$.

Without a detailed analysis which will be given in a forthcoming paper let us remark that the delimiter that forces u_t to 0 at some extrema never takes effect for $p \geq 1$ as in this case one has $u_t > 0$ ($u_t < 0$) in the surrounding regular points of minima (maxima). For $p < 1$ the lock-in at $u_t = 0$ first affects extrema where the Hessian of u is highly anisotropic (including curves consisting of extrema). As p decreases toward 0, this behaviour gradually extends to less anisotropic extrema. For $p < 0$, even isotropic critical points enter this regime such that now all local extrema develop into plateaus.

3 An L^∞ -stable Numerical Scheme for the PDE Limit

Our PDE limit (6) creates two major numerical difficulties:

- It involves the anisotropic expressions $u_{\xi\xi}$ and $u_{\eta\eta}$. To reproduce their qualitative properties adequately, one has to take care that the discretisation approximates rotationally invariant behaviour well and that it satisfies a discrete maximum–minimum principle which prevents over- undershoots.
- For $p < 1$, the sign in front of the operator $u_{\eta\eta}$ becomes negative, which results in a backward parabolic operator. Such operators are known to be ill-posed. They require additional stabilisation in the model and the numerics.

These challenges show that great care must be invested in the design of appropriate numerical algorithms. Thus, let us have a deeper look into our efforts along these lines.

Using $u_{\eta\eta} = \Delta u - u_{\xi\xi}$ and $u_{\xi\xi} = \text{curv}(u)|\nabla u|$ with the isophote curvature $\text{curv}(u)$ we rewrite (6) in a numerically more convenient form:

$$u_t = (2-p) \text{curv}(u)|\nabla u| + (p-1) \Delta u. \quad (21)$$

If $p \geq 1$, we apply this equation in all locations, including extrema.

For $p < 1$, the second term describes backward diffusion, which we stabilise by freezing its action in extrema where $|\nabla u|$ vanishes:

$$u_t = (2-p) \text{curv}(u)|\nabla u| + (p-1) \text{sgn}(|\nabla u|) \Delta u. \quad (22)$$

In practice, our image domain is finite and of rectangular size. This motivates us to equip the equations (21) and (22) with reflecting boundary conditions.

Both evolutions are replaced by explicit finite difference schemes on a regular grid of size h in x - and y -dimension and time step size τ . By $u_{i,j}$ we denote an approximation of u in pixel (i, j) .

If $p \geq 1$, we discretise Δu in (21) with a nine-point stencil that averages an approximation aligned along the x - and y -axis with one aligned along the diagonal directions:

$$\frac{1}{2} \frac{1}{h^2} \begin{array}{|c|c|c|} \hline 0 & 1 & 0 \\ \hline 1 & -4 & 1 \\ \hline 0 & 1 & 0 \\ \hline \end{array} + \frac{1}{2} \frac{1}{(\sqrt{2}h)^2} \begin{array}{|c|c|c|} \hline 1 & 0 & 1 \\ \hline 0 & -4 & 0 \\ \hline 1 & 0 & 1 \\ \hline \end{array} = \frac{1}{4h^2} \begin{array}{|c|c|c|} \hline 1 & 2 & 1 \\ \hline 2 & -12 & 2 \\ \hline 1 & 2 & 1 \\ \hline \end{array}. \quad (23)$$

This guarantees that all four principal grid directions are treated equally. Our experiments will also show that in this way, rotation invariance is approximated well.

For $p < 1$, the term $(p-1) \text{sgn}(|\nabla u|) \Delta u$ in (22) creates stabilised backward diffusion. Here we base our finite difference approximation on a minmod discretisation of Osher and Rudin [19], but average it again with its counterpart along the diagonal directions to guarantee equal treatment of the four principal grid directions. We denote the forward differences in x -, y -, and the diagonal directions $\mathbf{d} = (1, 1)$ and $\mathbf{e} = (1, -1)$ by

$$u_{i,j}^x := \frac{u_{i+1,j} - u_{i,j}}{h}, \quad u_{i,j}^y := \frac{u_{i,j+1} - u_{i,j}}{h}, \quad (24)$$

$$u_{i,j}^{\mathbf{d}} := \frac{u_{i+1,j+1} - u_{i,j}}{\sqrt{2}h}, \quad u_{i,j}^{\mathbf{e}} := \frac{u_{i+1,j-1} - u_{i,j}}{\sqrt{2}h}, \quad (25)$$

and abbreviate the minmod function by

$$M(a, b, c) := \begin{cases} a & \text{if } |a| = \min\{|a|, |b|, |c|\}, \\ b & \text{if } |b| = \min\{|a|, |b|, |c|\}, \\ c & \text{if } |c| = \min\{|a|, |b|, |c|\}. \end{cases} \quad (26)$$

With these notations we approximate $\operatorname{sgn}(|\nabla u|) \Delta u$ in pixel (i, j) by

$$\begin{aligned} & \frac{1}{2} \frac{1}{h} \left(M(u_{i+1,j}^x, u_{i,j}^x, u_{i-1,j}^x) - M(u_{i,j}^x, u_{i-1,j}^x, u_{i-2,j}^x) \right. \\ & \quad \left. + M(u_{i,j+1}^y, u_{i,j}^y, u_{i,j-1}^y) - M(u_{i,j}^y, u_{i,j-1}^y, u_{i,j-2}^y) \right) \\ & + \frac{1}{2} \frac{1}{\sqrt{2}h} \left(M(u_{i+1,j+1}^d, u_{i,j}^d, u_{i-1,j-1}^d) - M(u_{i,j}^d, u_{i-1,j-1}^d, u_{i-2,j-2}^d) \right. \\ & \quad \left. + M(u_{i+1,j-1}^e, u_{i,j}^e, u_{i-1,j+1}^e) - M(u_{i,j}^e, u_{i-1,j+1}^e, u_{i-2,j+2}^e) \right). \end{aligned} \quad (27)$$

Let us now discuss our approximation of $(2-p) \operatorname{curv}(u) |\nabla u|$. The isophote curvature

$$\operatorname{curv}(u) = \frac{u_x^2 u_{yy} - 2u_x u_y u_{xy} + u_y^2 u_{xx}}{(u_x^2 + u_y^2)^{3/2}} \quad (28)$$

can be discretised in a straightforward way with central differences. To avoid a potential singularity in the denominator, we regularise by adding $\epsilon = 10^{-10}$ to $u_x^2 + u_y^2$. Moreover, note that the isophote curvature $\operatorname{curv}(u)$ describes the inverse radius of the osculating circle to the level line. Since a discrete image does not have structures that are smaller than a single pixel, the smallest practically relevant radius is $\frac{h}{2}$. Thus, we impose a curvature limiter that restricts the computed result to the range $[-\frac{2}{h}, \frac{2}{h}]$.

Depending on the sign of $(2-p) \operatorname{curv}(u)$, we may interpret $(2-p) \operatorname{curv}(u) |\nabla u|$ either as a dilation term (for positive sign) or an erosion term (for negative sign) with a disc-shaped structuring element of radius $|(2-p) \operatorname{curv}(u)|$; see e.g. [1]. For a stable discretisation of $|\nabla u|$, we use the Rouy-Tourin upwind scheme [20]. In the dilation case, this comes down to

$$|\nabla u|_{i,j} \approx \sqrt{(\max(-u_{i-1,j}^x, u_{i,j}^x, 0))^2 + (\max(-u_{i,j-1}^y, u_{i,j}^y, 0))^2}, \quad (29)$$

and in the erosion case to

$$|\nabla u|_{i,j} \approx \sqrt{(\max(-u_{i,j}^x, u_{i-1,j}^x, 0))^2 + (\max(-u_{i,j}^y, u_{i,j-1}^y, 0))^2}. \quad (30)$$

Consistency. Since our resulting explicit scheme uses various one-sided – and thus first order – finite difference approximations within its upwind and minmod strategies, it follows that its general consistency order outside extrema is $\mathcal{O}(h + \tau)$. For the case $p = 2$, however, the second order stencil (23) gives $\mathcal{O}(h^2 + \tau)$.

Stability. All components of our explicit scheme are specifically selected to create a nonnegative approximation for an admissible time step size. This allows us to prove its L^∞ stability and a discrete maximum–minimum principle. Since the details are somewhat cumbersome and do not give more general insights, we sketch only the basic ideas by briefly analysing the contributions of the individual terms.

Let $\mathbf{u}^{k+1} = (\mathbf{I} + \tau \mathbf{A})\mathbf{u}^k$ be the matrix-vector notation of the explicit scheme for the diffusion evolution $u_t = \Delta u$. Here the vector \mathbf{u}^k contains the values of u in all pixels at time $k\tau$, \mathbf{I} is the unit matrix, and the matrix \mathbf{A} represents the discretisation of Δu with the stencil (23) and reflecting boundary conditions that are implemented by mirroring. Then all entries of the iteration matrix $\mathbf{I} + \tau \mathbf{A}$ are nonnegative, if $1 - \frac{12\tau}{4h^2} \geq 0$. This leads to the stability condition $\tau \leq \frac{h^2}{3}$ for the forward diffusion process. Following the arguments in [19], the same stability limit can also be derived for an explicit scheme for the stabilised backward diffusion process $u_t = -\text{sgn}(|\nabla u|)\Delta u$ that involves the minmod discretisation (27).

The explicit Rouy-Tourin scheme for the dilation/erosion evolutions $u_t = \pm|\nabla u|$ can be shown to be L^∞ -stable for $\tau \leq \frac{h}{2}\sqrt{2}$.

By combining all these restrictions in a worst case scenario, it follows that our explicit scheme for the full evolution equation (21) or (22) must satisfy the stability condition

$$\tau \leq \frac{h^2}{2\sqrt{2}|2-p| + 3|p-1|}. \quad (31)$$

It guarantees L^∞ stability and a discrete maximum–minimum principle. In practice this restriction is not very severe: With $h := 1$, it comes down to $\tau \leq \frac{1}{3}$ for the diffusion evolution ($p = 2$), to $\tau \leq \frac{1}{4}\sqrt{2} \approx 0.354$ for mean curvature motion ($p = 1$), and to $\tau \leq 0.069$ for the mode equation ($p = -1$). Thus, we can compute the PDE evolutions for M-smoothers not only in a stable way, but also fairly efficiently.

4 Experiments

In our experiments, we evaluate the PDE (6) with five different settings for p : a temporally rescaled midrange evolution ($p \rightarrow \infty$) using $u_t = u_{\eta\eta}$ with $\tau = 0.1$, the mean evolution leading to homogeneous diffusion ($p = 2$, $\tau = 0.25$), the median evolution yielding mean curvature motion ($p = 1$, $\tau = 0.25$), the mode evolution ($p = -1$, $\tau = 0.05$), and the Gabor flow ($p = -2$, $\tau = 0.04$).

Fig. 1 illustrates the effect of these equations on the real-world test image *trui*. The CPU times for computing each of these results on a contemporary laptop are in the order of half a second. We observe that the midrange filter produces fairly jagged results, although it has a clear smoothing effect. Homogeneous diffusion does not suffer from jagged artifacts, but blurs also important structures such as edges. The median evolution smoothes only along isolines which results in a smaller deterioration of edge-like structures. The mode and the Gabor evolutions are very similar and may even enhance edges due to their backward parabolic term $-u_{\eta\eta}$.

Fig. 2 allows to judge if our numerical algorithm is capable of reproducing the rotationally invariant behaviour of its underlying PDE (6). We observe excellent rotation invariance. Moreover, we see that the mode and Gabor evolutions have comparable shrinkage properties as mean curvature motion. However, they differ from mean curvature motion by their backward term $-u_{\eta\eta}$, which can compensate dissipative artifacts that are caused by the discretisations of the forward parabolic term.

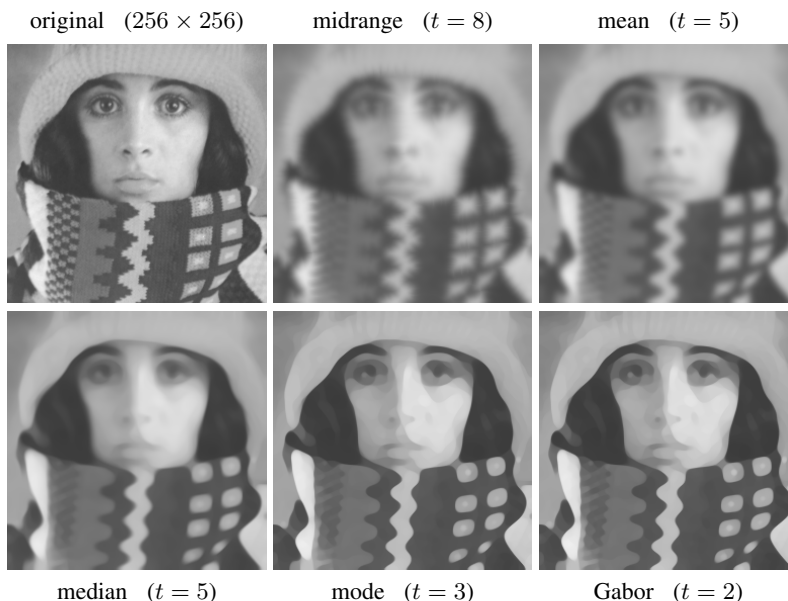


Fig. 1. Smoothing effect of the different evolution equations on the test image *trui*.

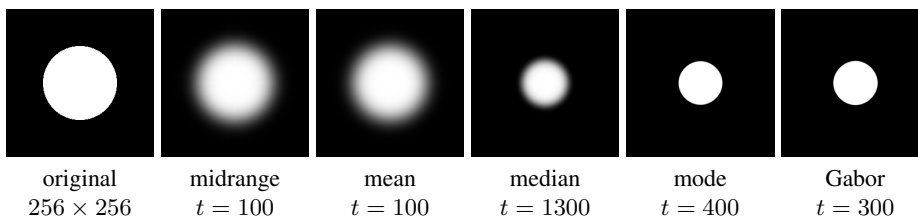


Fig. 2. Effect of the different evolution equations on a rotationally invariant test image.

In Fig. 3, we study the shape simplification properties of the mode evolution: It shrinks the binary shape of the kiwi in such a way that highly curved structures evolve faster than less curved ones, resulting in an evolution where nonconvex shapes become convex and vanish in finite time by shrinking to a circular point. Thus, the mode evolution appears to enjoy the same shape simplification qualities as mean curvature motion. However, that fact that it does not suffer from dissipative artifacts constitutes a distinctive advantage and makes it attractive for many shape analysis problems. Last but not least, Fig. 3 shows that the bird existed long before the egg, giving the ultimate answer to a deep problem in philosophy.

5 Summary and Conclusions

We have established a comprehensive analysis that identifies the PDE limit for the full class of iterated M-smoothers with order- p means. It does not only reproduce known

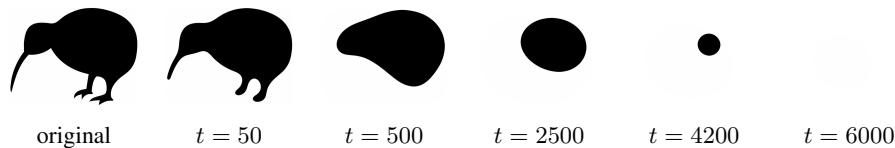


Fig. 3. Shape simplification properties of the mode evolution. Image size: 579×449 . Source of original image: https://commons.wikimedia.org/wiki/File:Kiwi_silhouette-by-flomar.svg.

results for mean and median filtering, but also corrects a common misconception in the literature: We have shown the surprising fact that in the continuous limit, mode filtering does not correspond to $p = 0$, but results from the limit $p \rightarrow -1$. Moreover, our filter class $u_t = u_{\xi\xi} + (p-1)u_{\eta\eta}$ can also be extended to models that have no interpretation within the setting of M-smoothers, e.g. Gabor’s classical method for $p = -2$.

Since literal implementations of some M-smoothers such as mode filtering can be highly nontrivial when using small local histograms [10, 14], we have proposed a novel numerical algorithm that can handle the PDE evolution for arbitrary p -values. Although these evolutions can be highly anisotropic and may even exhibit backward parabolic behaviour, we managed to come up with an L^∞ -stable finite difference scheme that is fairly efficient, satisfies a maximum–minimum principle and shows very good rotation invariance. This has been partly achieved by employing and adapting powerful stabilisation concepts from the numerics of hyperbolic PDEs, such as upwinding, minmod functions, and curvature limiters. Our numerical algorithm is applicable to any stable evolution of type $u_t = a u_{\xi\xi} + b u_{\eta\eta}$, where a and b may have arbitrary sign. Thus, it is of very general nature and covers also numerous applications beyond M-smoothing, including image interpolation [4], adaptive filter design [3], and many level set methods [18]. Exploring some of these applications is part of our ongoing work.

Our experiments indicate that the PDEs for $p < 1$, such as the mode evolution, are particularly appealing: They combine strong shape simplification properties with excellent sharpening qualities. They clearly deserve more research.

Connecting the class of M-smoothers to the family of PDE-based methods contributes one more mosaic stone to the mathematical foundations of image analysis. Since M-smoothers themselves are related to many other approaches [17, 23, 24], including W-smoothers, bilateral filters, mean-shift and robust estimation, our results can help to gain a broader and more coherent view on the entire field.

Acknowledgement. This project has received funding from the European Research Council (ERC) under the European Union’s Horizon 2020 research and innovation programme (grant agreement No. 741215, ERC Advanced Grant INCOVID).

References

1. Alvarez, L., Guichard, F., Lions, P.L., Morel, J.M.: Axioms and fundamental equations in image processing. *Archive for Rational Mechanics and Analysis* **123**, 199–257 (1993)
2. Barral Souto, J.: El modo y otras medias, casos particulares de una misma expresión matemática. Report No. 3, Cuadernos de Trabajo, Instituto de Biometría, Universidad Nacional de Buenos Aires, Argentina (1938)

3. Carmona, R., Zhong, S.: Adaptive smoothing respecting feature directions. *IEEE Transactions on Image Processing* **7**(3), 353–358 (Mar 1998)
4. Caselles, V., Morel, J.M., Sbert, C.: An axiomatic approach to image interpolation. *IEEE Transactions on Image Processing* **7**(3), 376–386 (Mar 1998)
5. Chu, C.K., Glad, I., Godtliebsen, F., Marron, J.S.: Edge-preserving smoothers for image processing. *Journal of the American Statistical Association* **93**(442), 526–556 (1998)
6. Fréchet, M.: Les éléments aléatoires de nature quelconque dans un espace distancié. *Annales de l'Institut Henri Poincaré* **10**, 215–310 (1948)
7. Gabor, D.: Information theory in electron microscopy. *Laboratory Investigation* **14**, 801–807 (1965)
8. Gauss, C.F.: *Theoria motus corporum coelestium in sectionibus conicis solem ambientium*. Perthes & Besser, Hamburg (1809)
9. Griffin, L.D.: Mean, median and mode filtering of images. *Proceedings of the Royal Society of London, Series A* **456**(2004), 2995–3004 (2000)
10. Griffin, L.D., Lillholm, M.: Mode estimation using pessimistic scale space tracking. In: Griffin, L.D., Lillholm, M. (eds.) *Scale-Space Methods in Computer Vision, Lecture Notes in Computer Science*, vol. 2695, pp. 266–280. Springer, Berlin (2003)
11. Guichard, F., Morel, J.M.: Partial differential equations and image iterative filtering. In: Duff, I.S., Watson, G.A. (eds.) *The State of the Art in Numerical Analysis*, pp. 525–562. No. 63 in *IMA Conference Series (New Series)*, Clarendon Press, Oxford (1997)
12. Huber, P.J.: *Robust Statistics*. Wiley, New York (1981)
13. Jackson, D.: Note on the median of a set of numbers. *Bulletin of the American Mathematical Society* **27**, 160–164 (1921)
14. Kass, M., Solomon, J.: Smoothed local histogram filters. *ACM Transactions on Graphics* **29**(4) (Jul 2010), article 100
15. Legendre, A.M.: *Nouvelles Méthodes pour la détermination des Orbites des Comètes*. Firmin Didot, Paris (1805)
16. Lindenbaum, M., Fischer, M., Bruckstein, A.: On Gabor's contribution to image enhancement. *Pattern Recognition* **27**, 1–8 (1994)
17. Mrázek, P., Weickert, J., Bruhn, A.: On robust estimation and smoothing with spatial and tonal kernels. In: Klette, R., Kozera, R., Noakes, L., Weickert, J. (eds.) *Geometric Properties from Incomplete Data, Computational Imaging and Vision*, vol. 31, pp. 335–352. Springer, Dordrecht (2006)
18. Osher, S., Paragios, N. (eds.): *Geometric Level Set Methods in Imaging, Vision and Graphics*. Springer, New York (2003)
19. Osher, S., Rudin, L.: Shocks and other nonlinear filtering applied to image processing. In: Tescher, A.G. (ed.) *Applications of Digital Image Processing XIV, Proceedings of SPIE*, vol. 1567, pp. 414–431. SPIE Press, Bellingham (1991)
20. Rouy, E., Tourin, A.: A viscosity solutions approach to shape-from-shading. *SIAM Journal on Numerical Analysis* **29**, 867–884 (1992)
21. Torroba, P.L., Cap, N.L., Rabal, H.J., Furlan, W.D.: Fractional order mean in image processing. *Optical Engineering* **33**(2), 528–534 (February 1994)
22. Tukey, J.W.: *Exploratory Data Analysis*. Addison–Wesley, Menlo Park (1971)
23. van den Boomgaard, R., van de Weijer, J.: On the equivalence of local-mode finding, robust estimation and mean-shift analysis as used in early vision tasks. In: *Proc. 16th International Conference on Pattern Recognition*, vol. 3, pp. 927–930. Quebec City, Canada (Aug 2002)
24. Winkler, G., Aurich, V., Hahn, K., Martin, A., Rodenacker, K.: Noise reduction in images: some recent edge-preserving methods. *Pattern Recognition and Image Analysis* **9**(4), 749–766 (1999)